J Appl Electrochem (2009) 39:135–140
DOI 10.1007/s10800-008-9645-9

ORIGINAL PAPER

Effect of the preparation conditions of carbon-supported Pt catalyst on PEMFC performance

Ji Bong Joo · Pil Kim · Wooyoung Kim · Younghun Kim · Jongheop Yi

Received: 1 May 2007 / Accepted: 24 July 2008 / Published online: 19 August 2008

Abstract Carbon-supported Pt catalysts were prepared using $NaBH_4$ as a reducing agent in either ethylene glycol or water for use as a cathode catalyst in PEMFCs (polymer electrolyte membrane fuel cells). Aqueous $NaBH_4$ solution was used to reduce Pt precursor and to produce the Pt-W catalyst, while Pt-E and Pt-E-base catalysts were synthesized using $NaBH_4$ in ethylene glycol for the reduction of Pt. Compared to Pt-W catalyst, Pt-E and Pt-E-base catalysts have higher Pt dispersion and larger EAS (electrochemically active surface area) due to the stabilizing effect of ethylene glycolic $NaBH_4$ solution on Pt particles. In addition, increasing pH of the preparation solution improved the Pt dispersion (Pt-E-base). In unit cell tests the performance of Pt catalysts decreased in the following order: Pt-E-base > Pt-E > Pt-commercial > Pt-W. Higher metal dispersion and larger EAS are believed to be responsible for the superior performance of Pt-E catalysts, particularly Pt-E-base, compared to other catalysts.

Keywords Supported Pt catalyst · pH · Dispersion · Ethylene glycol · PEMFC

J. B. Joo · W. Kim · J. Yi (✉)
School of Chemical and Biological Engineering, Institute of Chemical Processes, Seoul National University, Shinlim-dong, Kwanak-ku, Seoul 151-742, South Korea
e-mail: jyi@snu.ac.kr

P. Kim
School of Chemical Engineering & Specialized Graduate School of Hydrogen and Fuel Cell Engineering, Chonbuk National University, Deokjin-dong 1ga, Deokjin-ku, Jeonju 561-756, South Korea

Y. Kim
Department of Chemical Engineering, Kwangwoon University, Wolgye-dong, Nowon-gu, Seoul 139-701, South Korea

1 Introduction

PEMFCs (polymer electrolyte membrane fuel cells) are possible alternatives power sources for portable electronic devices, vehicles, and residential power generators, due to their high power density and low operating temperature [1–7]. Although considerable progress has been made in their commercialization over the past decade, many obstacles still remain to be overcome, including the high cost of the catalyst, which is based on precious metals [8]. To reduce the overall cost of PEMFCs, it is necessary to reduce the amount of Pt loaded on the MEA (membrane electrode assembly) without loss of unit cell performance. In addition, Pt particles in the catalyst should be small and well dispersed for the use of Pt more effectively [9–14].

In recent years various methods have been proposed for preparing highly dispersed Pt catalysts on carbon black [15–21]. The colloidal method, using organic stabilizers, has been widely used to produce supported Pt catalysts of small size and with homogeneous distribution [22, 23]: however, if preparation conditions are not optimized during Pt reduction it is difficult to reproduce the supported Pt catalyst with uniform distribution. Distinctive routes based on polyol and alcohol reduction methods have been recently developed with good results [9, 24–26]. In particular, Bock and co-workers successfully synthesized uniform Pt nanoparticles on carbon black using ethylene glycol [26]. In this process, in order to achieve uniform nanometer-sized particles, the solution temperature should be increased to 160 °C within a short period during the reduction of the Pt precursor. In the alcohol reduction method, surfactants with a high reduction temperature are required to reduce the Pt precursor [27, 28].

Another strategy for high metal dispersion is to control other synthetic conditions such as the amount of solvent

and the solution pH. Precious metal ions (i.e., Pt, Pd, and Au) are easily stabilized in the high pH range. Uniform Pt nanoparticles have been synthesized by using of due to the high electrosteric stabilization effect [29–32].

In this work, Pt catalysts were prepared using $NaBH_4$ in ethylene glycol solution as a reducing agent. The properties of the resulting Pt catalysts were controlled by changing the pH in the preparation solution. A highly dispersed carbon-supported Pt catalyst was successfully prepared at ambient conditions and used as a cathode catalyst in PEMFCs. The Pt catalysts were characterized by X-ray diffraction (XRD), transmission electron microscopy (TEM), and electrochemical methods.

2 Experimental

2.1 Catalyst preparation and characterization

$H_2PtCl_6 \cdot 6H_2O$ (Aldrich) and Vulcan XC-72 (Cabot Corp., $S_{BET} = 230\ m^2\ g^{-1}$) were used as a Pt precursor and carbon support, respectively. Figure 1 shows the preparation procedure of the Pt catalysts. Pt was reduced using a synthetic reducing agent produced by mixing ethylene glycol with $NaBH_4$ (see 'A' in Fig. 1). The typical preparation procedure was as follows. To prepare the reducing agent solution ethylene glycol was reacted with $NaBH_4$. The Pt precursor was dissolved in ethylene glycol (EG), and the carbon support was well dispersed in solution. This reducing agent solution (A) was slowly added to the above EG solution with vigorous stirring. After stirring for 6 h, diluted HCl solution was added for deposition of the Pt nanoparticles on the carbon support. The precipitate was filtered, washed with large amounts of de-ionized water, and dried at 120 °C overnight to give the final carbon-supported Pt catalyst (Pt-E: Pt catalyst prepared in ethylene glycol). In order to investigate the effects of preparation conditions, the pH of the ethylene glycol solution was raised to 11 and the Pt-E-base catalyst was obtained (Pt catalyst prepared in ethylene glycol at basic pH). For comparison a supported Pt catalyst was prepared by conventional sodium borohydride reduction using aqueous $NaBH_4$ solution (Pt-W). FE–SEM–EDX analyses showed that 40 wt% Pt was successfully loaded on the carbon support in all catalysts.

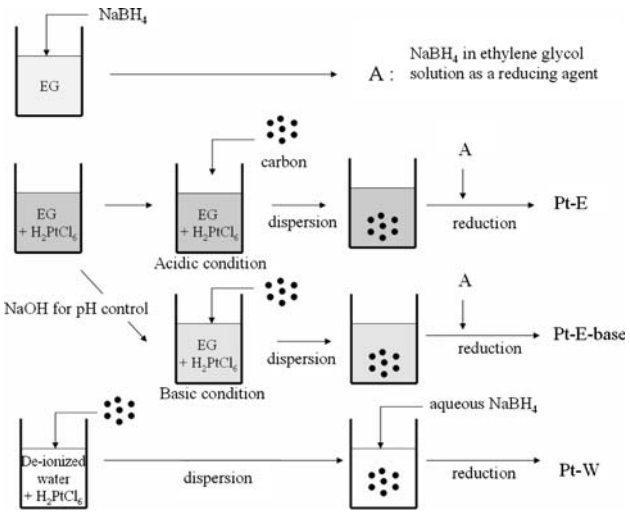

Fig. 1 Preparation procedure for the supported Pt catalysts. A: reducing agent produced using ethylene glycol with $NaBH_4$, Pt-W: Pt catalyst using aqueous $NaBH_4$ solution, Pt-E: Pt catalyst using reducing agent A, Pt-E-base: Pt catalyst using reducing agent A under basic pH conditions

2.2 Electrochemical analysis and single cell test

The electrochemically active surface areas (EASs) of the prepared catalysts were measured by cyclic voltammetry using an EG&G potentiostat. The cyclic voltammetry experiments were conducted in a conventional three-electrode system, with a saturated calomel electrode (SCE) and platinum gauze as the reference electrode and the counter electrode, respectively. The working electrode was prepared by coating the catalyst ink on disk-type graphite. Cyclic voltammograms (CVs) were obtained at room temperature at a scan rate of 20 mV s^{-1} in 0.5 M H_2SO_4 from −0.25 to 1.0 V vs. SCE. For CO-stripping voltammograms, CO was adsorbed to the surface of the working electrode by bubbling CO into the electrolyte of 0.5 M H_2SO_4 for 30 min, while holding the working electrode potential at −0.142 V vs. SCE. After CO bubbling, the gas was switched to nitrogen for 20 min and the potential was scanned from −0.25 to 1.0 V vs. SCE to record the CO-stripping voltammogram.

MEAs were prepared using the CCM (catalyst-coated membrane) method reported by Reshetenko et al. [33]. Nafion-112 (Dupont), pretreated by boiling in 3 wt% H_2O_2 and 0.5 M H_2SO_4, was used as a solid electrolyte. The catalyst ink was sprayed on the pretreated Nafion-112 membrane. The catalyst-coated membrane and commercial carbon papers (ETEK) as gas diffusion layers were assembled on both electrodes at ambient conditions without the hot-pressing process. The anode electrode contained a commercial 40 wt% Pt catalyst (Pt-commercial) with a metal loading of 0.2 mg Pt cm^{-2}, and the cathode electrode contained the prepared Pt catalysts with a metal loading of 0.35 mg Pt cm^{-2}, which was identical for all MEAs. A single cell test was conducted using a homemade PEMFCs test station. The geometric area of the electrode was 5 cm^2 and the cell was operated at 70 °C. Hydrogen as the anode fuel and oxygen at the cathode were fed at rates of 450 and 400 mL min^{-1}, respectively.

3 Results and discussion

Figure 2 shows the XRD patterns of Pt-E-base, Pt-E, Pt-W, and Pt-commercial with a loading of 40 wt% Pt. In all catalysts, a broad peak at ca. $2\theta = 25°$ was observed due to the (002) plane of the hexagonal structure of the carbon support, indicating that Vulcan XC-72 is amorphous carbon with small regions of graphitic properties [34]. Typical characteristic diffractions for the face-centered cubic phase of Pt were observed for all the catalysts. The average crystalline sizes of the Pt catalysts were calculated by the Scherrer formula based on the diffraction peaks of the Pt (220) plane. Surface areas of crystalline Pt were calculated from the crystalline size using the following equation:

$$S = \frac{6000}{\rho d},$$

where d is the average crystallite size (nm), S is the surface area ($m^2\ g^{-1}$) and ρ is the density of Pt (21.4 g cm^{-3}). The sizes and surface areas are summarized in Table 1.

The Pt-W catalyst prepared using $NaBH_4$ in water showed the largest crystallite size among the studied catalysts. The sizes of Pt-E-base and Pt-E, prepared using $NaBH_4$ in ethylene glycol solution as the reducing agent, were smaller than that of the Pt-commercial catalyst. It has been reported that the reaction of EG with $NaBH_4$ forms a complex reducing agent, and has performed roles as both a reducing agent for Pt reduction and a stabilizer for the reduced Pt nanoparticles [35]. Compared to Pt-E, the Pt-E-base catalyst had relatively highly dispersed Pt nanoparticles on the surface of the carbon support. Bönnemann et al. reported that Pt nanoparticles are stabilized via electrosteric repulsion between the anionic surface of the Pt nanoparticle and the stabilizer [36]. In acidic solution, a large number of H^+ ions interact with negatively charged Pt particles, resulting in the destruction of electrosteric repulsion and leading to the growth of Pt nanoparticles. In basic solution, almost no species would directly interact with negatively charged Pt nanoparticles, implied that the electrosteric stabilization is unbroken [32, 36–38].

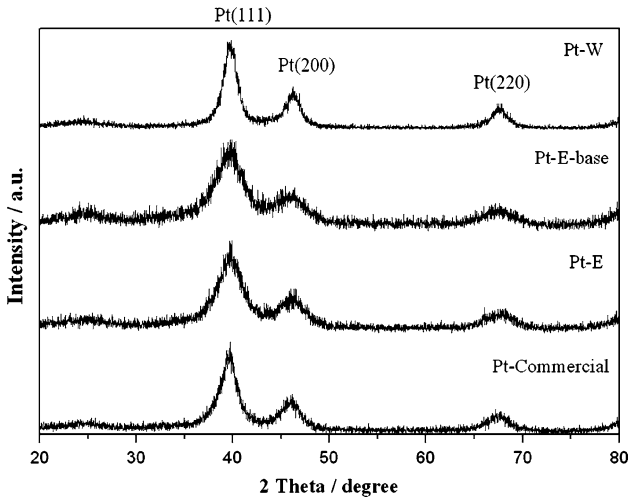

Fig. 2 XRD patterns of the supported Pt catalysts

A similar feature has also been observed in the synthesis of Pt-based metal nanoparticles using EG as a reducing agent [25, 26]. In our case, the differences in Pt particles between Pt-E and Pt-E-base can also be explained by the effect of electrosteric repulsion. Under high-pH conditions, only minor interaction occurred between H^+ ions and stabilizer anions, yet the stabilizer interacted strongly with the reduced Pt nanoparticles. Therefore, the growth of Pt particles was suppressed, leading to the formation of Pt nanoparticles with smaller size in the Pt-E-base than in the Pt-E catalyst.

Figure 3 shows TEM images of the Pt catalysts. The Pt-W catalyst has the largest size of Pt on the carbon support among the employed Pt catalysts. Pt-E-base and Pt-E have higher metal dispersion than Pt-commercial, and Pt-E-base has slightly smaller Pt particles than Pt-E (in high-magnification TEM images). These features are consistent with the results of XRD analyses.

Figure 4 shows CVs for the prepared Pt catalysts in acidic electrolyte (0.5 M H_2SO_4), which were used to estimate EAS using the Coulombic charge for H^+ ion adsorption–desorption. The CVs of the Pt catalysts show four different characteristic regions: a typical proton ion adsorption–desorption region, a double-layer charging current region, a Pt pre-oxidation region, and a Pt reduction region. The peak area for the H^+ ion adsorption–desorption current is proportional to EAS values, which were calculated from the integrated average charges after correction for the contribution of the double-layer charging current [39–42]:

$$S_{\mathrm{EAS-H}} = \frac{Q_{\mathrm{H}}}{0.21 \times [\mathrm{Pt}]},$$

where S_{EAS-H}, Q_H, and [Pt] are the EAS value ($m^2\ g_{Pt}^{-1}$), average Coulombic charge for H^+ ion adsorption–desorption (C), and platinum loading (mg cm^{-2}), respectively. The resultant EAS values are listed in Table 1. S_{EAS-H} values decreased in the following sequence: Pt-E-base > Pt-E > Pt-commercial > Pt-W. This trend also corresponds with the results of TEM and XRD analyses.

The EAS was further confirmed via CO-stripping voltammetry, as shown in Fig. 5. A representative CO-stripping voltammogram of the Pt-commercial catalyst is shown in the inset image in Fig. 5. In the first cycle, the peak at 0.47 V vs. SCE represents the electro-oxidation of irreversibly adsorbed CO on the Pt surface. The calculated peak charge, Q_{CO}, is related to the CO oxidation reaction [39, 40].

Table 1 Average crystallite size calculated from the Pt (220) using the Scherrer equation, surface areas calculated from the Pt crystalline size (S_{XRD}) and electrochemically active surface area (EAS) by H^+ ion adsorption (S_{EAS-H}) and by CO adsorption (S_{EAS-CO})

	Average crystallite size (nm)	S_{XRD} ($m^2\ g_{Pt}^{-1}$)	S_{EAS-H} ($m^2\ g_{Pt}^{-1}$)	S_{EAS-CO} ($m^2\ g_{Pt}^{-1}$)
Pt-W	4.9	57	25	20
Pt-E	3.0	93	92	80
Pt-E-base	2.6	108	109	94
Pt-commercial	3.6	77	60	55

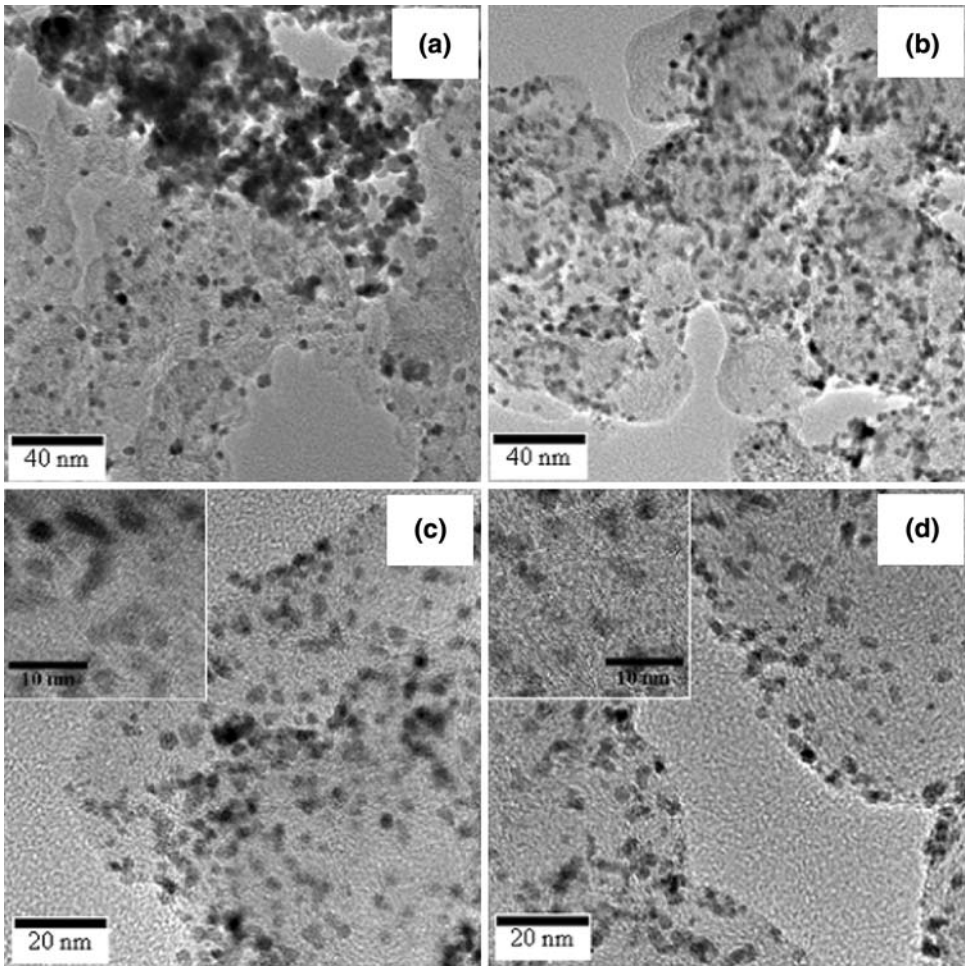

Fig. 3 TEM images of the supported Pt catalysts: (**a**) Pt-W, (**b**) Pt-commercial, (**c**) Pt-E, and (**d**) Pt-E-base

$$Pt - CO + H_2O \rightarrow Pt + CO_2 + 2e^- + 2H^+$$

The peak charge of CO oxidation, Q_{CO}, can be used to calculate the EASs of the prepared Pt catalysts using the following equation:

$$S_{EAS-CO} = \frac{Q_{CO}}{0.484 \times [Pt]},$$

where the value 0.484 represents the charge density required to oxidize a monolayer of CO on the Pt surface [40]. The S_{EAS-CO} values obtained by CO-stripping voltammetry are listed in Table 1. The S_{EAS-CO} values were lower than the S_{EAS-H} values; however, the trends in S_{EAS-CO} value are identical to those in S_{EAS-H} and Pt surface area calculated from XRD results. The TEM, XRD, and CV data indicate that the preparation method that employs $NaBH_4$ in ethylene glycol solution as a reducing agent under basic conditions is highly favorable for the formation of finely dispersed Pt nanoparticles on the carbon support.

Figure 6 shows the cell polarization curves for PEMFCs and maximum power densities of the supported Pt catalysts at 70 °C. Because an identical catalyst was used in all cases with the same loading of Pt catalyst on the anode electrode, the differences in cell performances are mainly attributed to catalytic activities in the cathodes. As shown in Fig. 6a, the order of cell performances of the prepared Pt catalysts

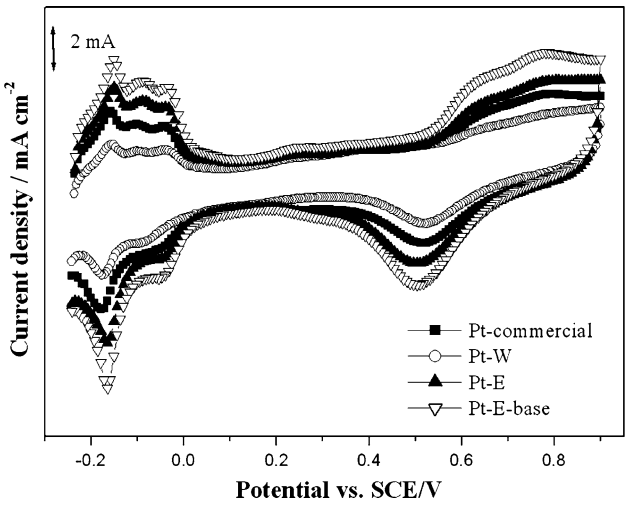

Fig. 4 Cyclic voltammograms of the supported Pt catalysts

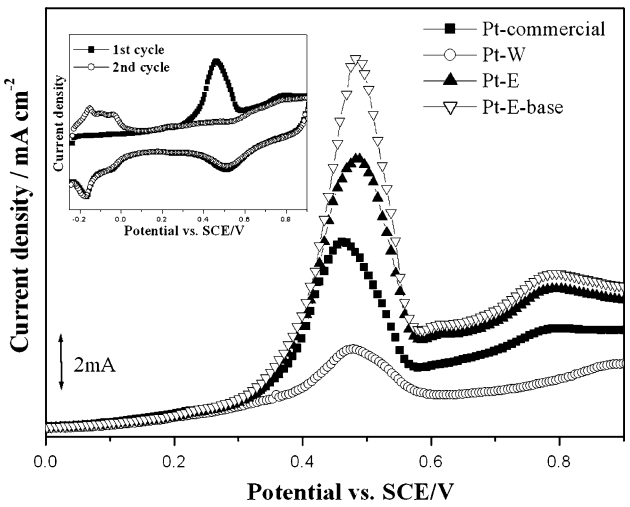

Fig. 5 Representative CO-stripping voltammogram of Pt-commercial catalyst (inset image) and CO-oxidation peaks of the supported Pt catalysts

is as follows: Pt-W < Pt-commercial < Pt-E < Pt-E-base. At a current density of 1.2 A cm^{-2}, the cell potentials of Pt-W, Pt-commercial, Pt-E, and Pt-E-base were 0.26, 0.52, 0.56, and 0.61 V, respectively. Compared to Pt-commercial, Pt-E-base exhibits higher maximum power density by a factor of 1.25; Pt-W shows the lowest cell performance.

As previously observed, good dispersion of active metal particles may affect catalytic performance for oxygen electro-reduction in PEMFCs [41–43]. Because electrochemical reactions in a fuel cell occur at the interface between the fuel, the catalyst and the electrolyte (i.e., a three-phase boundary), highly dispersed Pt particles produce the many sites required for electro-catalysis [42–46]. Therefore, the remarkable cell performance of Pt-E-base is

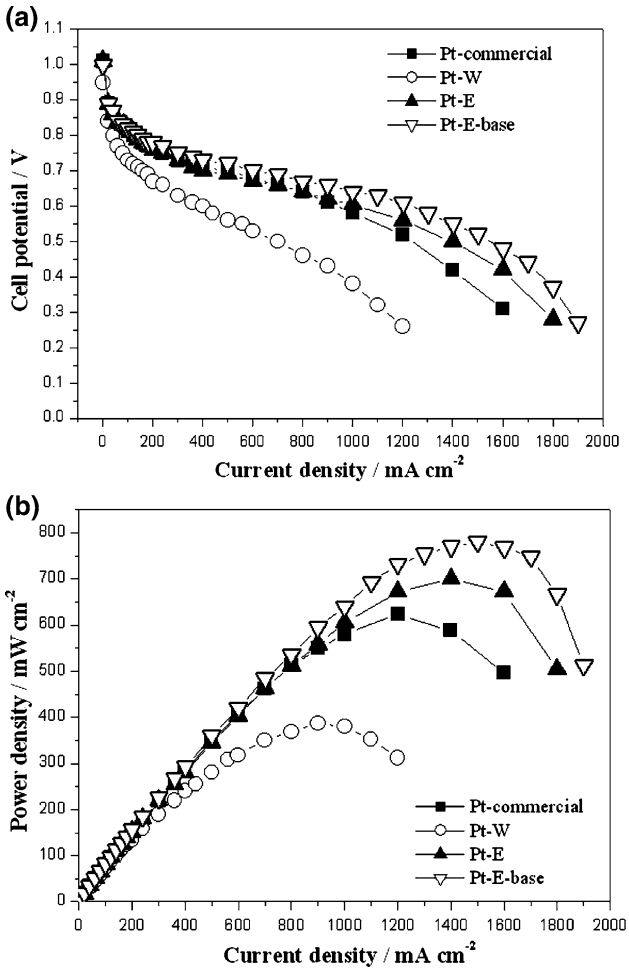

Fig. 6 (**a**) Cell polarization curves and (**b**) maximum power densities of the supported Pt catalysts

probably attributable to the fact that it yields the highest EAS.

4 Conclusions

A carbon-supported Pt catalyst was prepared using $NaBH_4$ in ethylene glycol solution. Compared to Pt-W and Pt-commercial catalysts, the Pt catalysts (Pt-E and Pt-E-base) prepared using $NaBH_4$ in ethylene glycol solution show high metal dispersion. The highest Pt dispersion was obtained in solution of high pH due to electrosteric stabilization between the small Pt nanoparticles and stabilizer. In unit cell tests for PEMFC, the highest cell performance was observed when using the Pt-E-base catalyst. It is thought that the enhanced catalytic activity results from the fact that Pt-E-base has the highest EAS among the prepared Pt catalysts.

Acknowledgment This work was supported by Grant No. R01-2006-000-10239-0 from the Basic Research Program of the Korea Science & Engineering Foundation.

References

1. Gasteiger HA, Kocha SS, Sompalli B et al (2005) Appl Catal B 56:9
2. Rastler D (2000) J Power Sources 86:34
3. Bernay C, Marchand M, Cassir M (2002) J Power Sources 108:139
4. Wee J-H (2007) Renew Sust Energy Rev 11:1720
5. Silva RF, Francesco MD, Giorgi L et al (2004) J Solid State Electrochem 8:544
6. Roth C, Goetz M, Fuess H (2001) J Appl Electrochem 31:793
7. Shafia Hoor F, Ahmed MF, Mayanna SM (2004) J Sol State Electrochem 8:572
8. Steele BCH, Heinzel A (2001) Nature 414:345
9. Wang X, Hsing IM (2002) Electrochim Acta 47:2981
10. Ismagilov ZR, Kerzhentsev MA, Shikina NV et al (2005) Catal Today 102–103:58
11. Mizuhata H, S Nakao, Yamaguchi T (2004) J Power Sources 138:25
12. Gulla AF, Saha MS, Allen RJ et al (2006) J Electrochem Soc 153:A366
13. Benítez R, Soler J, Daza L (2005) J Power Sources 151:108
14. Martz N, Roth C, Fueß H (2005) J Appl Electrochem 35:85
15. Tamai H, Nakatsuchi S, Kera Y et al (2003) J Mater Sci Lett 22:145
16. Tian JH, Wang FB, Shan ZQ et al (2004) J Appl Electrochem 34:461
17. Li W, Liang C, Zhou W et al (2003) J Phys Chem B 107:6292
18. Zhou Z, Wang S, Zhou W et al (2003) Phys Chem Chem Phys 5:5485
19. Chen WX, Lee JY, Liu Z (2002) Chem Commun 21:2588
20. Liu H, Song C, Zhang L et al (2006) J Power Sources 155:95
21. Zhang X, Chan KY (2003) Chem Mater 15:451
22. Castro Luna AM, Camara GA, Paganin VA et al (2000) Electrochem Commun 2:222
23. Paulus UA, Endruschat U, Feldmeyer GJ et al (2000) J Catal 195:383
24. Liu Z, Hong L, Tham MP et al (2006) J Power Sources 161:831
25. Zhou Z, Zhou W, Wang S et al (2004) Catal Today 93–95:523
26. Bock C, Paquet C, Couillard M et al (2004) J Am Chem Soc 126:8028
27. Liu Z, Gan LM, Hong L et al (2005) J Power Sources 139:73
28. Yu W, Tu W, Liu H (1999) Langmuir 15:6
29. Kim T, Takahashi M, Nagai M et al (2004) Electrochim Acta 50:817
30. Liu Z, Tian ZQ, Jiang SP (2006) Electrochim Acta 52:1213
31. Li X, Chen W-X, Zhao J et al (2005) Carbon 43:2168
32. Hui CL, Li XG, Hsing IM (2005) Electrochim Acta 51:711
33. Reshetenko TV, Kim H-T, Lee H et al (2006) J Power Sources 160:925
34. Zhou WJ, Li WZ, Song SQ et al (2004) J Power Sources 131:217
35. Kim P, Joo JB, Kim W et al (2006) J Power Sources 160:987
36. Bönnemann H, Braun G, Brijoux W et al (1996) J Organomet Chem 520:143
37. Li X, Hsing IM (2006) Electrochim Acta 51:5250
38. Oh H-S, Oh J-G, Hong Y-G et al (2007) Electrochim Acta 52:7278
39. Vielstich W, Lamm A, Gasteiger H (2003) Handbook of fuel cells: fundamentals, technology, applications, vol 2. Wiley, New York
40. Pozio A, De Francesco M, Cemmi A et al (2002) J Power Sources 105:13
41. Perez J, Gonzalez ER, Ticianelli EA (1998) Electrochim Acta 44:1329
42. Tamizhmani G, Dodelet JP, Guay D (1996) J Electrochem Soc 143:18
43. Joo JB, Kim P, Kim W et al (2006) Catal Today 111:171
44. Kim M, Park J-N, Kim H et al (2006) J Power Sources 163:93
45. Liu C, Xue X, Lu T et al (2006) J Power Sources 161:68
46. Shao Y, Yin G, Wang J et al (2006) J Power Sources 161:47